Available online at www.sciencedirect.com
SCIENCE DIRECT
International Journal of Heat and Mass Transfer 49 (2006) 3957–3967
International Journal of HEAT and MASS TRANSFER
www.elsevier.com/locate/ijhmt

A steady state model and maximum heat transport capacity of an electrohydrodynamically augmented micro-grooved heat pipe

Balram Suman *

Department of Chemical Engineering and Materials Science, 151 Amundson Hall, 421 Washington Avenue, SE, University of Minnesota, Minneapolis, 55455 MN, USA
School of Mathematics, University of Minnesota, Minneapolis, 55455 MN, USA

Received 6 November 2005; received in revised form 4 April 2006
Available online 16 June 2006

Abstract

A model for the fluid flow and heat transfer in an electrohydrodynamically (EHD) augmented micro-heat pipe is presented utilizing a macroscopic approach. Coulomb and dielectrophoretic forces have been considered in the model. The coupled non-linear governing equations for the fluid flow, heat and mass transfer are developed based on the first principles and are solved numerically. The effects of Coulomb and dielectrophoretic forces have been studied together and the effects have been compared. The analytical expressions for the critical heat input and for the dry-out length have been obtained, which show that with an increase in the electric field intensity, the critical heat input increases and the dry-out length decreases. It is found that using EHD, the critical heat input can be increased by 100 times. The contribution of Coulomb force is observed stronger than that of dielectrophoretic force. Also, the critical heat input and the dry-out length have been successfully compared with the experimental results available in the literature. The general nature of the model and the associated parametric study will be useful to understand the EHD pumping in a micro-heat pipe.

Keywords: Micro-heat pipe; Electrohydrodynamics; Capillary force; Critical heat input; Dry-out length

1. Introduction

The micro-scale heat exchange is an active area of research due to its possible potential applications in electronic cooling, thermal treatment of some diseases, temperature management in fuel cell, microgravity environments, and space craft thermal control [1–4]. The micro-grooved heat pipe is widely acceptable because of its simple design and direct integration on the substrate. In a micro-grooved heat pipe, the flow of liquid is due to the difference in the radius of curvature between the hot end and the cold end. One of the factors that limit the heat transport capacity of a micro-heat pipe is the large viscous losses associated with the transport of the coolant liquid from the condenser to the evaporator [5,6]. Therefore, its heat transport capacity is less than that of a wicked heat pipe. Several attempts have been made in the past to increase the heat transport capacity of a heat pipe [7–13]. These methods have been compared [13]. The arterial modification was proven successful and other experienced problems associated with vibrations and/or size limitations. The electrohydrodynamic (EHD) pumping is new and offers a promise to improve the heat transport capacity of a micro-heat pipe. Only the EHD-assisted heat pipe provides an overall mass saving, which is a prime NASA concern [14]. It is more useful where space limitation is the main issue like laptop computer and other small electronic devices.

The micro-heat pipe, as first proposed by Cotter [15], is defined to be so small that the mean curvature of the liquid–vapor interface is necessarily comparable in

* Address: Department of Chemical Engineering and Materials Science, Mailbox # 30, 151 Amundson Hall, 421 Washington Avenue, SE, University of Minnesota, Minneapolis, 55455 MN, USA. Tel.: +1 612 624 1828; fax: +1 612 626 7246.
E-mail address: suman@cems.umn.edu

0017-9310/$ - see front matter © 2006 Elsevier Ltd. All rights reserved.
doi:10.1016/j.ijheatmasstransfer.2006.04.011

Nomenclature

a	side length of a V-groove, m
A_{cs}	area of cross-section of substrate, m^2
A_g	vapor cross-section area, m^2
A_l	liquid cross-section area, m^2
A_t	V-groove cross-section area, m^2
B_l	constant in expression for A_l
B_2, c	constant
Bo	Bond number
C_{pl}	specific heat of the coolant liquid, J/(kg °C)
C_{ps}	specific heat capacity of the substrate, J/(kg °C)
D_h	hydraulic diameter, m
d_l	liquid hydraulic diameter, m
d_v	vapor liquid diameter, m
E	electric field, N/C
Fe	electrical force, N
f	friction factor
g	acceleration due to gravity, m/s^2
K'	constant in expression for B_2
K_s	thermal conductivity, W/(m °C)
L	length of heat pipe, m
L_h	half of total wetted length, m
L_l	effective liquid length, m
L_v	effective vapor length, m
N_{Re}	Reynolds number
P_l	liquid pressure, N/m^2
P_l^*	non-dimensional liquid pressure
P_R	reference pressure, N/m^2
P_{vo}	pressure in vapor region, N/m^2
ΔP_{EHD}	available pressure due to electrohydrodynamic pumping, N/m^2
ΔP_c	available pressure due to capillary, N/m^2
ΔP_g	available pressure due to gravity, N/m^2
ΔP_l	pressure loss due to liquid flow, N/m^2
ΔP_v	pressure loss due to vapor flow, N/m^2
q	charge, C
Q	heat flux supplied to the coolant liquid, W/m^2
Q^l	heat supplied to the coolant liquid, W
Q_v	heat flux for at the interface, W/m^2
R	radius of curvature, m
R_h	radius of curvature, m
R^*	non-dimensional radius of curvature
R_0	reference radius of curvature, m
R_l	meniscus surface area per unit length, m
R_e	radius of curvature at the hot end, m
T_{con}	temperature at the cold end, °C
T_l	temperature of the coolant liquid, °C
T_l^*	dimensionless temperature of the coolant liquid
T_R	reference temperature, °C
T_s	temperature of substrate, °C
T_s^*	dimensionless substrate temperature
V	potential, V
V_g	axial vapor velocity, m/s
V_l	axial liquid velocity, mm/s
V_l^*	non-dimensional liquid velocity
V_g^*	non-dimensional vapor velocity
V_R	reference liquid velocity, m/s
W_b	V-groove pitch, m
x	coordinate along the heat pipe, m
X^*	non-dimensional coordinate along heat pipe

Greek symbols

α	half groove angle, rad
β	inclination of substrate, rad
γ	contact angle, rad
ε	permittivity, $C^2/N\ m^2$
ε_0	absolute permittivity, $C^2/N\ m^2$
ε_l	liquid permittivity, $C^2/N\ m^2$
ε_v	vapor permittivity, $C^2/N\ m^2$
ϕ	curvature, m^{-1}
λ_l	latent heat of vaporization of coolant liquid, J/kg
μ_l	viscosity of coolant liquid, kg/m s
ρ	charge density, C/m^3
ρ_0	charge density in coolant liquid, $Coulomb/m^3$
ρ_l	density of coolant liquid, kg/m^3
ρ_s	density of substrate, kg/m^3
ρ_v	density of vapor, kg/m^3
σ_l	surface tension of coolant liquid, N/m
τ_w	wall shear stress, N/m^2

magnitude to the reciprocal of the hydraulic radius of the total flow channel. It should be distinguished from a miniature heat pipe which has a larger hydraulic radius to liquid–vapor interface curvature ratio. A typical micro-heat pipe has a hydraulic diameter ranging from 10 μm to several millimeters and a length of up to several centimeters. By definition, a micro-heat pipe requires the Bond number ($Bo = \frac{\rho_l g R_h^2}{\sigma_l}$) to be of the order of less than or equal to one. Several steady state models for a micro-heat pipe have been presented in literature [16–29]. These models have used Young–Laplace equation to relate liquid and vapor pressure using curvature of the liquid menisci.

The EHD pumping results from the application of an electric field to a dielectric fluid. It has a number of advantages over other active techniques in enhancing a micro-heat pipe performance: (i) does not require much space; (ii) simple design, non-mechanical, and lightweight; (iii) rapid control of enhancement; (iv) suitable for special environments (space); (v) minimal power consumption; (vi) applicable to single or two phase flows; (vii) uniform pressure distribution across pumping section and (viii) temperature and heat to be transported, is tunable. But, the implementation of the EHD phenomena to fluid dynamics and heat transfer introduces a complex interaction of many

interdependent variables. These variables are (i) electrical and thermophysical fluid properties; (ii) electrical field strength; (iii) fluid medium, single or multi-phase; (iv) geometry of micro-heat pipe; (v) geometry and configuration of electrodes; (vi) properties of electrodes and insulators; and (vii) operating environment.

Few researchers have attempted to improve the heat transport of a heat pipe using EHD phenomena. Jones [30] proposed to replace the capillary wick structure in a heat pipe with an EHD pump that utilized polarization forces to generate pumping. Jones and Perry [31] used the EHD heat pipe successfully, but the performance was poorer than the existing capillary driven heat pipe. Loehrke and Debs [32] improved the electrohydrodynamic (EHD) heat pipe of Jones and Perry and were able to achieve equivalent thermal performance of conventional axial-groove heat pipes. Bologa and Savin [33] used the dielectrophoretic force to enhance the heat transport capacity in an experimental heat pipe operating as a two-phase thermosiphon and obtained 53% increase in the heat transport capacity after using 36 kV. The enhancement of the heat pipe transport capacity utilizing the coulomb force was investigated by Babin et al. [34]. They used an ion-drag pump to generate the Coulomb force and to increase the capillary limit of the heat pipe. They have also mentioned that the ion-drag pumps are capable of providing continuous pumping and require a low power input. They have power efficiency of approximately 5–10% and appear to be well suited as an alternate active pumping mechanism for a micro-heat pipe. Sato et al. [35] proposed the use of the electrostriction force to generate pumping to increase the heat pipe capillary limit, but did not provide any experimental evidence. Melcher [36] discussed the phenomena that dielectric liquid tended to fill the region where the electric field is the strongest. Bryan and Seyed-Yagoobi [37] performed an experimental study on a monogroove EHD heat pipe and obtained 100% increment in the heat transport capacity. Hallinan and his co-workers [38,39] proposed an analytical model of an EHD-assisted micro-heat pipe, which can be used to predict the maximum heat transport capacity and the optimum geometry. They have obtained six times increase in the heat transport capacity. They have used electric field to enhance the heat capacity of a heat pipe using electrodes. Their electrode pair sandwiched the groove in the evaporator section. The electrodes were directly attached to the 1-mm-thick cover slide adhered to the open side of the grooves. This way, the electrode was in intimate contact with the liquid. The ground electrodes were attached to the exterior surface of the grooved slide. Therefore, the spacing between two electrodes of different levels was very small ($\sim$1 mm). The electrodes were fashioned out of aluminum foil. The application of the high voltage across the electrodes was achieved using a high-voltage dc power supply. The voltage was monitored using a high-voltagemeter. Later, Yu et al. [40] presented a semi empirical model of a system cooled by a micro-heat pipe array that will permit analytical investigation of the efficacy of employing an electric field in response to heat input variations.

Thus in recent years there has been a great interest in EHD pumping heat pipes. The mathematical modeling of EHD assisted micro-heat pipe is a way to start to understand it and is further important in the design and optimization of a heat pipe. A mathematical model for the fluid flow and heat transfer of an EHD assisted micro-heat pipe is yet to be developed. Comparison between the benefits of the Coulomb and dielectrophoretic forces has not been reported. First of all heat pipe limits, the capillary limit reaches in most of real life applications. The theoretical calculation of the dry-out length has not been addressed for an EHD assisted micro-heat pipe. Therefore, an important extension of the EHD assisted micro-heat pipe research will involve modeling of the heat, mass and momentum transfer in an electrodynamically augmented micro-heat pipe considering the Coulomb and dielectrophoretic forces and obtaining the analytical expressions for the critical heat input and for the dry-out length. This extension of the EHD assisted micro-heat pipe research has been the subject of this work. Finally, the experimental results have been successfully compared with the results available in the literature.

2. Theory

The system being studied herein is a V-shaped micro-grooved micro-heat pipe, though the model equations are general in nature in terms of the shape of the grooves. The micro-heat pipe is inclined at an angle to provide a body force. Due to capillary pumping, the liquid will be pushed towards the hot end. The liquid will travel along the corners and the vapor passes through the open space (Fig. 1). The hot and the cold end denote the farthest end of evaporative and the condenser region, respectively. The heat flux interaction between the substrate and the coolant liquid in the evaporative and the condenser regions is considered to be of constant value.

The dielectrophoretic force in an EHD micro-heat pipe has been designed to augment the liquid flow from the condenser to the evaporator. This force results from application of an electric field at a liquid–vapor interface. The physical explanation of the force derived from the polarizing effect of the electric field, which is greater in the liquid phase due to the larger electrical permittivity. When an

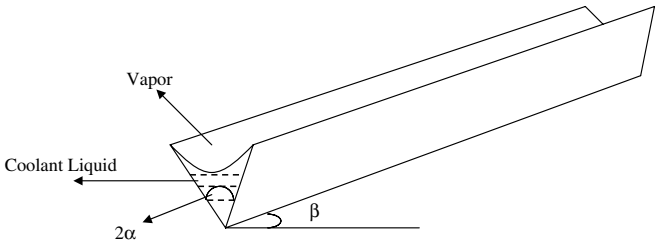

Fig. 1. Schematic of a V-shaped micro-heat pipe.

electric field is applied, the molecules of the dielectric field present within the micro-heat pipe are polarized and dipoles are formed. In the electric field, the dipoles are formed and other polarized molecules tend to become statistically more ordered and, therefore, exhibit a minimum-energy state. Therefore, the liquid tends to flow in the regions of higher electric field intensity due to the requirement of minimizing energy.

The EHD phenomenon involves the interaction of the electrical field and the flow field in a dielectric fluid medium. This interaction can result in electrically induced fluid motion that is caused by an electrical body force. The electrical body force acting on the molecules of a dielectric fluid in the presence of an electric field consists of three terms. Mathematically, it is given as [41]:

$$F_e = qE - \frac{1}{2}E^2\nabla\varepsilon + \frac{1}{2}\nabla\left[E^2\left(\frac{\partial\varepsilon}{\partial\rho}\right)\rho\right]. \quad (1)$$

In Eq. (1), the force due to electric field has been related to three different kinds of forces. The first term on the right hand side represents the Coulomb force, which acts on the free charges in an electric field. The second term on the right hand side stands for the dielectrophoretic force, which is created by a local change of the permittivity in an electric field. A change in the permittivity occurs at the interface between a liquid and a vapor. The third term on the right hand side is called the electrostriction force. The electrostriction force occurs primarily when a non-uniform electric field is applied on a dielectric fluid. The dielectrophoretic and the electrostriction forces act on polarized charges and are called as polarization forces. In the present model, first and second terms of right hand side have been utilized. Both terms (for Coulomb force and dielectrophoretic force) promote the flow of coolant liquid from the cold end to the hot end.

The model equations are developed for all three regions, i.e., evaporative, adiabatic and condenser encompassing the complete heat pipe. The governing model equations are derived under the following assumptions. (i) One dimensional steady incompressible flow along the length of a heat pipe, since the flow along the transition region is small [42]. (ii) Negligible heat dissipation due to viscosity. (iii) One dimensional temperature variation along the length of a heat pipe. (iv) Negligible shear stress at the liquid vapor interface because the channel area for vapor flow is relatively large and at the low heat fluxes used in this study, the vapor velocity will generally be small. This justifies the assumption of no shear stress at the liquid vapor interface [20]. (v) Predefined heat flux interaction between the substrate and the coolant liquid (Q) with position. The fluid flow is governed by the pressure difference between the hot and the cold ends. The vapor pressure also affects the evaporation and condensation. However, a successful formulation of dependency of heat fluxes on vapor pressure has not been done. Therefore, in this work the predefined heat flux interaction between the substrate and the coolant liquid has been considered similar to the one used in [23,25]. (vi) Convective heat loss has been neglected since two phase heat transfer is orders of magnitude higher than the natural convection. (vii) Disjoining pressure has not been considered. (viii) Constant pressure in the vapor region. The constant pressure in the vapor region assumption is valid in this case, as the vapor flow space in the channels is quite large especially considering the low heat fluxes used in this study. The vapor pressure drop required for flow has been calculated and was found to be very small. (ix) Uniform electric field is considered. However, it is difficult to maintain the uniform electric field in an EHD assisted heat pipe. The magnitude of the force due to non-uniform field is small because the force depends on the rate of change of electric field with position and the rate of change of permittivity with charge density. The permittivity change due to the charge density is small and hence, the force due to the non-uniform electric field is expected to be small, provided the rate of change of electric field is not large.

A V-shaped micro-heat pipe of length Δx is shown in Fig. 2 with all forces specified. The liquid pressure as a function of the radius of curvature can be estimated from the Young–Laplace equation, which is given in differential form as follows:

$$\frac{dP_l}{dx} = \frac{\sigma_l}{R^2}\frac{dR}{dx}. \quad (2)$$

The terms $\frac{dP_l}{dx}$ and $\frac{dR}{dx}$ are the pressure and the radius of curvature gradients, respectively. The steady state momentum balance in differential form is given as

$$\rho_l A_l V_l \frac{d(V_l)}{dx} + A_l\frac{dP_l}{dx} + 2L_h\tau_w - \frac{1}{2}E^2(\varepsilon_v - \varepsilon_l)\frac{dA_l}{dx} + A_l\rho_0 E - \rho_l g\sin(\beta)A_l = 0. \quad (3)$$

The first term in the above equation represents the convective momentum change, the second term is the pressure force acting on the volume element, the third term represents the wall shear force, the fourth term is the dielec-

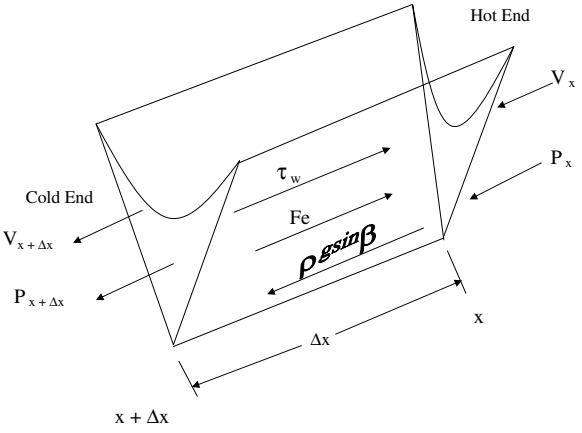

Fig. 2. Volume element of a V-shaped micro-heat pipe with all forces specified.

trophoretic force, the fifth term is the Coulomb force and the sixth term is the gravity force. The electric field and the maximum charge density in the liquid are given by Crowley's formula [43]:

$$E = \frac{\varepsilon_s V}{\varepsilon_l h + a[\varepsilon_s - \varepsilon_l]}, \tag{4}$$

$$\rho_0 \leqslant \left(\frac{2\varepsilon_l V}{h^2}\right), \tag{5}$$

where $h = R\left[\frac{\cos(\alpha+\gamma)}{\tan\alpha} + \sin(\alpha+\gamma) - 1\right]$.

The detail derivation of h is given in [44].

The differential form of the mass balance is given as

$$\frac{d}{dx}(\rho_l V_l A_l) + \frac{Q_v R_l}{\lambda_l} = 0. \tag{6}$$

The first term is the difference in the convective flow of liquid and the second term is the amount of liquid evaporated from the differential volume. The quantity R_l is the meniscus surface area per unit length of a heat pipe.

The mass flow across the heat pipe is zero and therefore, the expression for the vapor velocity can be given as

$$V_v = -\frac{\rho_l A_l V_l}{\rho_v A_v}. \tag{7}$$

The energy balance equation for the coolant liquid, after considering the sensible heat change in the volume element, is given as

$$\rho_l C_{pl} V_l A_l \frac{dT_l}{dx} = QW_b - Q_v R_l, \tag{8}$$

where Q is the heat flux interaction between the coolant liquid and the substrate. The quantity Q is positive when added (in the evaporative section) and is negative when extracted (in the condenser section). The quantity R_l is the meniscus surface area per unit length of a heat pipe.

The steady state energy balance in the substrate is given as

$$A_{cs} K_s \frac{d^2 T_s}{dx^2} - QW_b = 0, \tag{9}$$

where the first term is the net change in the heat conduction in the control volume and the second term is the heat interaction between the substrate and the coolant liquid.

2.1. Boundary conditions

There is no evaporation after the hot end of a heat pipe ($x = 0$), and hence, the liquid velocity is zero at the hot end. The radius of curvature at the hot end is given by Ma and Peterson [45]. Here the fluid flow is governed by the electrostatic forces and hence the curvature at the hot end does not have much effect. Hence, the radius of curvature at the hot end, R_e, is taken as 0.05 of the reference radius of curvature. The coupled differential and algebraic equations (2)–(9) can be solved by using the following boundary conditions:

$$\begin{aligned} \text{At } x = 0, \quad & V_l = 0, \\ & R = R\_e = 0.05 R_0, \\ & P_l = P_{vo} - \frac{\sigma_l}{R\_e} - \frac{1}{2}E^2(\varepsilon_l - \varepsilon_v), \\ & Q_{heater} = -K_s A_{cs} \left.\frac{dT_S}{dx}\right|_{x=0}. \end{aligned} \tag{10}$$

$$\text{At } x = L, \quad T_S = T_{con}. \tag{11}$$

2.2. Non-dimensionalization

The following non-dimensional and associated parameters have been used: friction factor $(f) = \frac{K'}{N_{Re}}$, Reynolds number $(N_{Re}) = \frac{D_h \rho_l V_l}{\mu_l}$, hydraulic diameter $(D_h) = \frac{4A_l}{2L_h}$, wall shear stress $(\tau_w) = \frac{\rho_l V_l^2 f}{2}$, shear at the liquid–vapor interface reference velocity $(V_R) = \frac{Q'}{\rho_l R_0^2 \lambda_l}$, reference pressure, $(P_R) = \frac{\sigma_l}{R_0}$, reference temperature $(T_R) = T_{con}$ and R_0 is taken as the side length of a V-groove. This is different from our previous work [26–29] since here the fluid flow is not only because of the capillary pressure, but also because of the electric forces and therefore, the scaling has been changed.

The dimensionless parameters are defined as follows: dimensionless radius of curvature $(R^*) = \frac{R}{R_0}$, dimensionless position $(X^*) = \frac{x}{L}$, dimensionless liquid velocity $(V_l^*) = \frac{V_l}{V_R}$, dimensionless vapor velocity $(V_g^*) = \frac{V_g}{V_R}$, dimensionless liquid pressure $(P_l^*) = \frac{P_l}{P_R}$, dimensionless substrate temperature $(T_s^*) = \frac{T_s}{T_R}$. The quantity K' is used in the expression of the friction factor (f), which is a constant for a specific geometry [46]. The final set of non-dimensionlized equations are as follows:

$$\frac{dR^*}{dX^*} = \frac{\left[\rho_l g \sin\beta - \rho_0 E + \frac{Q_v V_R R_l V_l^*}{A_l \lambda_l} - \frac{B_2 V_R V_l^*}{(R_0 R^*)^2}\right]}{\left[\frac{\sigma_l}{R_0 L R^{*2}} - \frac{2\rho_l V_R^2 V_l^{*2}}{L R_0} - \frac{E^2(\varepsilon_v - \varepsilon_l)}{L R^*}\right]}, \tag{12}$$

$$\frac{dV_l^*}{dX^*} = -\left[\frac{Q_v R_l L}{\rho A_l \lambda V_R} + 2\frac{V_l^*}{R^*}\frac{dR^*}{dX^*}\right], \tag{13}$$

$$\frac{dP^*}{dX^*} = \frac{\sigma}{R_0 P_R R^{*2}}\frac{dR^*}{dX^*}, \tag{14}$$

$$V_v^* = -\frac{\rho_l A_l V_l^*}{\rho_v A_v}, \tag{15}$$

$$Q_V = \frac{1}{R_l}\left[QW_b - \frac{\rho_l C_{Pl} V_R A_l V_l^*}{L}\frac{dT_l}{dX^*}\right], \tag{16}$$

$$Q = \frac{Q'}{fW_b L}, \tag{17}$$

$$\frac{d^2 T_s^*}{dX^{*2}} - \frac{QW_b L^2}{T_R A_{cs} K_s} = 0, \tag{18}$$

Eqs. (12)–(18) are valid for all three sections of a heat pipe namely, evaporative, adiabatic and condenser. The quantity Q is zero in the adiabatic section, negative in the condenser section (heat is extracted) and is positive in the evaporative section (heat is supplied). These equations can be solved numerically taking a predefined heat flux (Q), which is being transferred between the coolant liquid and the substrate.

The geometrical parameters A_l, W_b, and B_2 are taken from Suman et al. [27], taking zero ungrooved area. They are given as

$$\alpha = \frac{\pi}{6}, \tag{19}$$

$$A_l = R^2\left[\{\cot(\alpha+\gamma) - \phi/2\} + \frac{\cot(\alpha+\gamma)\cos(\alpha+\gamma)\sin\gamma}{\sin\alpha}\right], \tag{20}$$

$$A_v = A_t - A_l, \tag{21}$$

$$W_b = 2a, \tag{22}$$

$$R_0 = a, \tag{23}$$

$$B_2 = \frac{\mu_l K' \cos^2(\alpha+\gamma)}{2\sin^2\alpha\left[\frac{\cot(\alpha+\gamma)\cos(\alpha+\gamma)\sin\gamma}{\sin\alpha} + \{\cot(\alpha+\gamma) - \phi/2\}\right]^2}. \tag{24}$$

The dimensionless boundary conditions can be written as follows:

At cold end $(X^* = 0)$,

$$R^* = \frac{R\_e}{R_0} = 0.05,$$
$$V_l^* = 0,$$
$$P_l^* = \frac{P_{vo}}{P_R} - \frac{R_0}{R\_e} - \frac{1}{2P_R}E^2(\varepsilon_l - \varepsilon_v),$$
$$Q_{heater} = -\frac{K_s A_{cs} T_R}{L}\left.\frac{dT_S^*}{dX^*}\right|_{X^*=0}. \tag{25}$$

At hot end $(X^* = 1)$, $T_S^* = \frac{T_{con}}{T_R}$. (26)

of less than 1.0×10^{-3}. It is confirmed that the obtained result is independent of the step size. The reliability of numerical solution has been confirmed by reproducing results of [26].

2.4. Critical heat input and dry-out length

The critical heat input for a micro-heat pipe is the heat input when the pressure difference required for the fluid flow in a heat pipe is equal to the available pressure due to the capillary and the electrohydrodynamic pumping. The pressure balance equation at the critical heat input is given as

$$\Delta P_c + \Delta P_{EHD} = \Delta P_g + \Delta P_l + \Delta P_v, \tag{27}$$

$$\Delta P_c = \frac{\sigma_l}{R\_e} - \frac{\sigma_l}{R_0}, \tag{28}$$

$$\Delta P_{EHD} = -\frac{1}{2}E^2(\varepsilon_v - \varepsilon_l) + \rho_0 EL, \tag{29}$$

$$\Delta P_g = \rho_l g L\sin(\beta). \tag{30}$$

The pressure gradient in the liquid and the vapor passage is given by Chi [47], which are as follows:

$$\Delta P_l = \frac{128\mu_l L_l}{\pi d_l^4 \rho_l \lambda_l} Q, \tag{31}$$

$$\Delta P_v = \frac{2fL_v}{d_v^2 \rho_v^2 \lambda_v^2} Q^2. \tag{32}$$

Solving Eqs. (27)–(32), the expression for the critical heat input is given as

$$Q_{cr} = \frac{-128\mu_l L_l + \sqrt{(128\mu_l L_l)^2 - 8fL_v\left(\frac{\pi d_l^4\rho_l}{d_v\rho_v}\right)^2\left(\rho_l g L\sin(\beta) + \frac{1}{2}E^2(\varepsilon_v - \varepsilon_l) - \rho_0 V - \left(\frac{\sigma_l}{R\_e} - \frac{\sigma_l}{R_0}\right)\right)}}{\frac{4fL_v\pi d_l^4\rho_l}{d_v^2\rho_v^2\lambda_l}}. \tag{33}$$

2.3. Numerical solution

The coupled model equations are solved numerically. The inputs are Q-distribution for the evaporative and the condenser regions, geometry of the heat pipe, contact angle for the substrate and coolant liquid combination and thermophysical properties of the coolant liquid. First of all, the second order differential equation (18) has been solved independently since it is decoupled with other equations to obtain the substrate temperature profile. Finite difference technique is used to discretize and a tridiagonal matrix has been obtained. The axial coordinate has been discretized into 40-coupled non-linear equations. The equations are further solved by using Gauss–Seidel method. Then, model equations (12)–(17) are solved using Runge–Kutta fourth-order integration routine. A variable step size has been taken for the above iteration with the largest step size

The quantity ΔP_v is small compared to ΔP_l. Neglecting ΔP_v and using $L_l = L$, Q_{cr} becomes:

$$Q_{cr} = \frac{\pi d_l^4 \rho_l \lambda_l\left(-\rho_l g L\sin(\beta) - \frac{1}{2}E^2(\varepsilon_v - \varepsilon_l) + \rho_0 V + \left(\frac{\sigma_l}{R\_e} - \frac{\sigma_l}{R_0}\right)\right)}{128\mu_l L}. \tag{34}$$

The expression for the critical heat input in Eq. (34) has been used in this work. The value of R_e has been taken as $0.05R_0$ for the critical heat input calculation.

When the heat input is higher than the critical heat input, the flow of fluid required for evaporation and condensation is not met and then, a portion of the heat pipe becomes dry. The length of the dry-region is known as dry-out length. The dry-out length propagates from the hot end towards the cold end. Using Eq. (27), the dry-out length (L_d) for a set of process variables can be

obtained. While finding the critical heat input, length of a heat pipe is taken as a known variable and the value of the heat input is obtained, which is termed as critical heat input. In the same way, for a given heat input, the largest length of the heat pipe can be obtained. If the length of heat pipe is higher than the largest length of the heat pipe, the difference in the two lengths will give the dry-out length. Neglecting ΔP_v and using $L_l = L$, the expression for the dry-out length is obtained utilizing the above methodology, which is given as

$$L_d = L - \frac{\left(\frac{\sigma_l}{R_{-e}} - \frac{\sigma_l}{R_0}\right) - \frac{1}{2}E^2(\varepsilon_v - \varepsilon_l)}{\rho_l g \sin(\beta) - \rho_0 E + Q\frac{128\mu_l}{\pi d_l^4 \rho_l \lambda_l}}. \quad (35)$$

3. Results and discussion

A V-shaped micro-heat pipe has been considered here to present a model for the fluid flow and heat transfer in an electrohydynamically augmented micro-heat pipe. The silicon substrate is 0.8 cm wide and 3.1 cm long. 0.3 cm of this length is not grooved and is used by the heater to supply heat to the system. Hence, the effective length of the heat pipe is 2.8 cm. The lengths of the evaporative, the adiabatic and the condenser sections have been assumed to be equal. The V-groove width and the groove spacing are taken as 0.1 mm and the apex angle of a V-groove is 60°. The temperature at the condenser end and the reference temperature have been taken as 32 °C. The inclination of the micro-heat pipe is 10°. The 0.5 W heat input for 3 V-grooves has been taken. The thermophysical properties of the coolant liquid used in the numerical calculations have been presented in Table 1.

The radius of curvature has an important role, when a micro-heat pipe operates because of capillary pumping. The profiles of the radius of curvature along the length of the heat pipe for different electric field strengths have been presented in Fig. 3. The radius of curvature is increasing from the hot end to the end of the adiabatic section. Therefore, in this portion of the heat pipe, the capillary pressure also promotes the flow of coolant liquid. At the beginning of the condenser section, the condensation of the vapor starts and therefore, the mass flow rate of the coolant liquid decreases. But, due to the external electrical forces, the liquid velocity does not decrease so fast. This

Table 1
Thermophysical properties of a coolant fluid

Thermophysical quantities	Numerical values
ρ_l	636 kg/m^3
ρ_v	2.5 kg/m^3
σ_l	0.0171 N/m
μ_l	0.000259 kg/m s
λ_l	377,800 J/kg
γ	0 rad
ε_l	$1.8341\varepsilon_0$ C^2/N m^2
ε_v	ε_0 C^2/N m^2

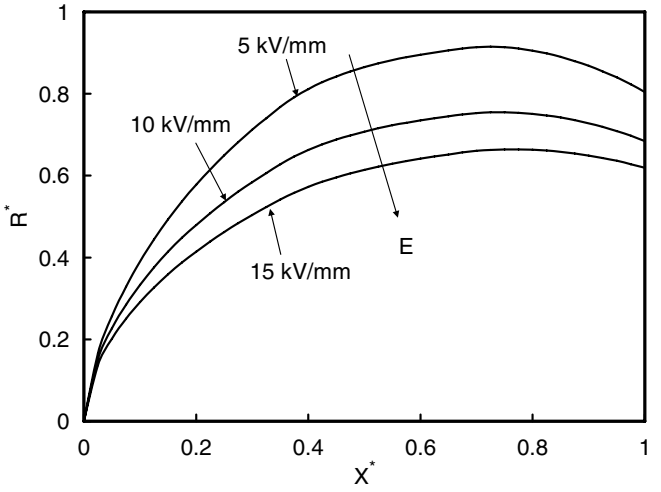

Fig. 3. Variation of the dimensionless radius of curvature (R^*) with the dimensionless axial position (X^*) with different electric field strength.

results into a decrease in the coolant liquid flow area and hence, we have decrease in the radius of curvature in the condenser section. It is also obtained that with an increase in the electric field intensity; the increase in the radius of curvature is also less. This is because that lesser is the electric field intensity; higher is the capillary pumping required for the fluid flow. This results into a higher radius of curvature at the cold end.

The variation of the magnitude of the liquid velocity is presented in Fig. 4. The calculated value of the axial liquid velocity from the simultaneous solution of the governing equations is negative due to the coordinate system used herein (origin at the hot end). The absolute value of the axial liquid velocity is zero at the hot end and increases in the evaporative region. The sharp increase in the liquid velocity at the hot end is because of a very low value of the radius of curvature. The increase in the liquid velocity

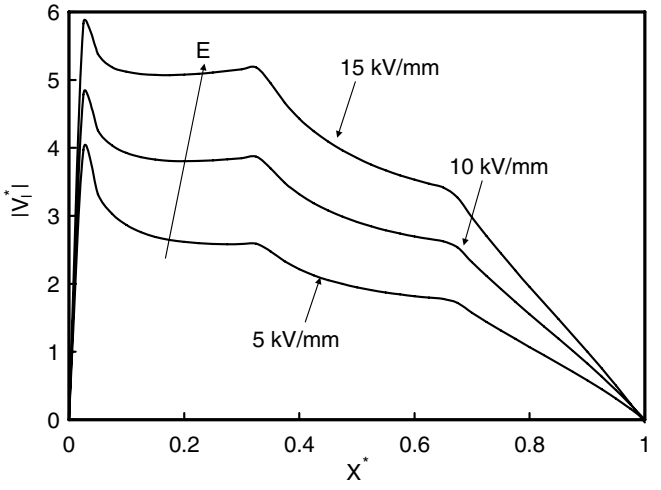

Fig. 4. Variation of the magnitude of dimensionless axial liquid velocity (V_l^*) with the dimensionless axial position (X^*) with different electric field strengths.

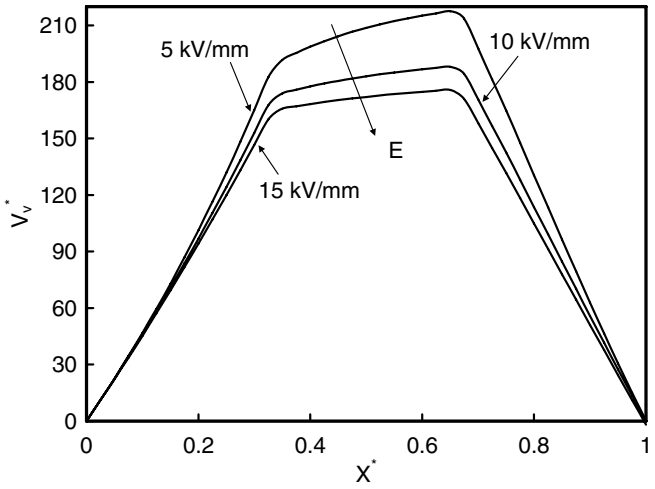

Fig. 5. Variation of the dimensionless axial vapor velocity (V_v^*) with the dimensionless axial position (X^*) with different electric field strengths.

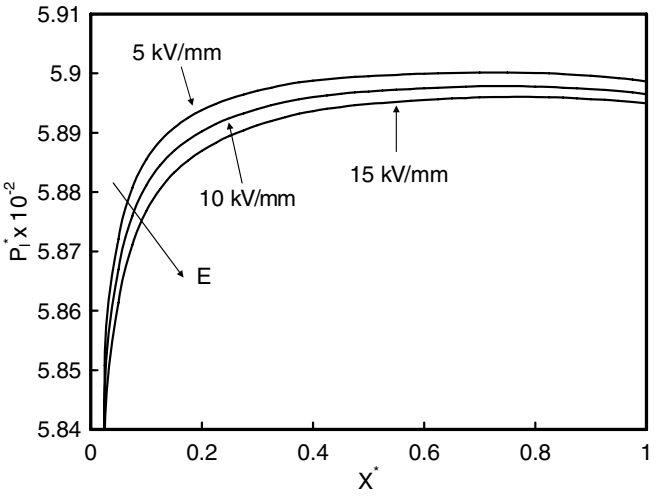

Fig. 6. Variation of the dimensionless liquid pressure (P_l^*) $\times 10^{-2}$ with the dimensionless axial position (X^*) with different electric field strengths.

is due to the cumulative effect of replenishing the amount evaporated throughout the evaporator region. Even though there is no evaporation and condensation in the adiabatic region, the liquid velocity still decreases. This is consistent with the increase in the radius of curvature in the adiabatic section (and hence an increase in the liquid flow area). In the condenser region, there is a further fall of the liquid velocity since the condensation results into a sharp increase in the value of radius of curvature. It can also be observed in Fig. 4 that with an increase in the electric field intensity, the liquid velocity increases. This is because of the higher electrical forces, which promote the flow from the cold end to the hot end. This can also be explained using Fig. 3. In Fig. 3, the radius of curvature is smaller for a higher electric field intensity and hence from the continuity equation, the velocity should be higher for a higher electric field.

The mass flow rate (flow rate of liquid + flow rate of vapor) at any cross-section of a micro-heat pipe is zero. The mass conservation equation (15) gives the vapor velocity in a heat pipe. It is important to calculate to check the sonic limit for a proper operation of a heat pipe. It is seen that the vapor velocity is much below the sonic velocity in all cases. The vapor velocity along the length of a heat pipe has been presented in Fig. 5. The direction of vapor velocity is from the hot end to the cold end. It has the similar trend as that of the magnitude of the liquid velocity in evaporative and condenser sections, which is expected. In the adiabatic section, the radius of curvature increases and area available for the vapor flow decreases. Therefore, a slight increase in the vapor velocity has been obtained. The magnitude of the vapor velocity is more than that of the liquid velocity since the density of the vapor is lower than that of the liquid. With an increase in the electric field, the vapor velocity decreases. This is because of lower radius of curvature (refer to Fig. 3) with a higher electric field and hence, higher vapor flow area.

The liquid pressure along the axial length of the heat pipe has been presented in Fig. 6. The liquid pressure is more at the cold end and less at the hot end. The difference in the liquid pressure between the hot end and the cold end is due to the change in the liquid menisci curvature along the length of a heat pipe. It is also found that with a lower electric field, the liquid pressure is higher is at the cold end so that the coolant liquid flows towards the hot end. This is because that at a lower electric field, higher capillary pressure is required and the pressure at the hot end is fixed and hence, the liquid pressure at the cold end is increased.

A part of the total heat supplied to the heat pipe is used by the liquid to raise the liquid temperature while remaining is used for evaporation. Only a small fraction of the heat input is used to increase the sensible heat of the coolant liquid. It is found that the amount of heat used for the sensible heat is negligible compared to the heat used for the evaporation and the condensation, which is in agreement with previous results published in the literature [42]. Hence, the sensible heat has a negligible effect on the heat pipe performance. The heat flux at the liquid–vapor interface (Q_v), which is a function of position is presented in Fig. 7. In the evaporative region, the evaporation of coolant liquid takes place and so it has a positive value. No evaporation and condensation take place in the adiabatic region and hence Q_v is zero. In the condenser region, the condensation of the coolant liquid takes place and therefore, it is negative. With an increase in the electric field, Q_v increases. This is because that R_l decreases with a higher electric field. Near the hot end, Q_v is high because the meniscus area is very small.

The critical heat input is the maximum heat transport capacity of a heat pipe. In Table 2, the critical heat inputs for different electric field strengths have been presented. They have been reported taking both electrical forces together and separately. The critical heat input values reported in the literature [26,28,29] for a micro-heat pipe

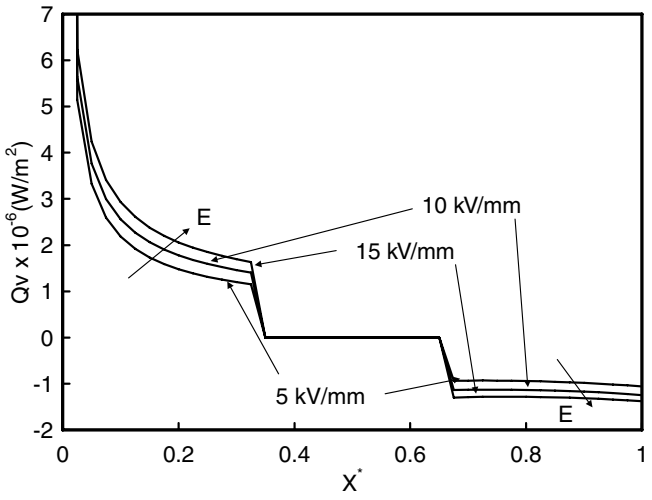

Fig. 7. Variation of $Q_v \times 10^{-6}$ (W/m^2) with the dimensionless axial position (X^*) with different electric field strengths.

Table 2
Variation of the critical heat input (W) with the electric field intensity (kV/mm)

Electric field (kV/mm)	Calculated critical heat input (W) using both effects	Calculated critical heat input (W) taking Coulomb force only	Calculated critical heat input (W) taking dielectrophoretic force only
2	1.58	1.57	0.34
4	2.86	2.81	0.37
6	4.15	4.05	0.43
8	5.47	5.3	0.51
10	6.81	6.54	0.69

without an electric field. They are of the order of 10^{-2}. On the other hand, from Table 2 it is seen that the critical heat input is of the order of one. Hence, it can be concluded that using an electric field, the heat transport capacity can be improved by 100 times. The heat transport capacity can be improved more using Coulomb force than that using dielectrophoretic force. This is because that Coulomb force acts on complete volume of the coolant liquid, which pulls the liquid to move towards the hot end. On the other hand, the dielectrophoretic force is due to change in permittivity and acts at the liquid vapor interface surface, which pushes the coolant liquid to move from the cold end to the hot end.

In the study of Yu et al. [39], the micro-heat pipe array has been used. It has been from a 1-mm-thick glass, 28 mm long and composed of 7 parallel grooves that terminated in plenums on both ends. The grooves and plenums were machined using an ultrasonic milling process. The cross-section of each channel was 1 mm wide by 0.6 mm deep, and the spacing between the channels was 1 mm. The working fluid was pentane, a dielectric fluid with a high vapor pressure. The heat pipe inclination was 9 degree. In Table 3, the model predicted critical heat input has been compared with the experimental results obtained by Yu et al. [39]. The experimental and the model predicted values are in good agreement. The minimum error is 2% with 5 kV/mm and 6 kV/mm and the maximum error is 20% with 8 kV/mm. The experimental value for 8 kV/mm seems to be lower in comparison with other data points. It is evident that the predicted values are higher than the experimental values since the pressure drop due to vapor has been neglected.

Table 3
Comparison between the experimental [39] and the theoretical critical heat input (W)

Electric field (kV/mm)	Calculated critical heat input (W)	Experimental critical heat input [39] (W)
4	2.32	2.0
5	2.56	2.5
6	2.86	2.8
7	3.21	3.0
8	3.62	3.2
9.5	4.32	4.1

The analytical expression developed for the dry-out length has been used to calculate a dry-out length for different heat inputs. They have been reported in Table 4, considering both electrical forces together as well as separately. The dry-out length is lower for Coulomb force than that with dielectrophoretic force. This is because Coulomb force acts on complete volume of the coolant liquid, which pulls the liquid to move towards the hot end. On the other hand, the dielectrophoretic force is due to change in permittivity and acts at the liquid vapor interface surface, which pushes the coolant liquid to move from the cold end to the hot end. It can also be said that at a higher heat input, the dry-out length is roughly the same for Coulomb force and dielectrophoretic force. This is because, when the amount of the coolant liquid in the heat pipe is less, the charge is less and therefore, the Coulomb force is less. It is obtained that the dry-out length is always smaller when both electrical forces are considered. This is because both electrical forces are available for the coolant liquid flow from the cold end to the hot end. It is to be noted that the contribution of two electrical forces are not additive since they are coupled using the radius of curvature.

Table 4
Variation of the dry-out length (mm) with the heat input (W) for a heat pipe of length 28 mm and electric field strength 10 kV/mm

Heat input (W)	Dry-out length (mm) using both effects	Dry-out length (mm) taking Coulomb force only	Dry-out length (mm) taking dielectrophoretic force only
7	6.4	16.0	25.5
8	18.4	22.7	25.8
9	21.8	24.6	26.1
10	23.4	25.5	26.8
11	24.4	26.0	26.4
12	25.0	26.4	26.6

Table 5
Comparison between the experimental [24] and the theoretical dry-out length (in mm) without electric field

Power (W)	Inclination (°)	Calculated dry-out length (mm)	Experimental dry-out length [24] (mm)	T_{amb} (°C)
1.52	43.16	14.8	14.2	35.0
1.71	38.66	15.92	16.5	32.6
1.71	90.00	15.95	16.5	32.6

In the study by Anand et al. [24], experiments were carried out in a specially designed cell to study the onset and propagation of a dry out point on a micro-grooved silicon surface with pentane as the coolant liquid. Chemical machining method was used to fabricate V-shaped axial micro-grooves on a silicon substrate. 33 V-grooves of 2 cm length with groove depth of 68.82 μm were used together with the top most groove depth of 100 μm and a groove pitch of 200 μm. Controlled heat was supplied on the top of the substrate and the axial temperature distribution was accurately measured as a function of input heat and inclination of the substrate. The comparison between the dry (without liquid) and wet (with liquid) temperature profiles were used to locate the dry-out point and its propagation as a function of inclination and supplied heat input. The comparison of the calculated and the experimental dry-out length is presented in Table 5. It may be observed from the table that the model predicted values of dry out length are in very good agreement with the experimental data. The error is around 5%. Thus the relatively simple analytical expression for the dry-out length, proposed in this study, correctly predicts the dry-out length.

4. Conclusions

A model for the fluid flow and heat transfer in an electrohydrodynamically augmented micro-heat pipe is presented utilizing a macroscopic approach. Coulomb and dielectrophoretic forces have been considered in the model. The coupled non-linear governing equations for the fluid flow, heat and mass transfer are developed based on the first principles and are solved numerically. The contributions of Coulomb and dielectrophoretic forces have been studied together and separately. The analytical expressions for the critical heat input and the dry out length have been obtained. It is observed that with an increase in the electric field intensity, the critical heat input increases and the dry-out length decreases. The critical heat input can be increased by 100 times using an electric field. The dry-out length increases with an increase in heat input, viscosity and friction factor. The effect of Coulomb force is found stronger than dielectrophoretic force. The critical heat input and the dry-out length values obtained using the expression developed in this work have been successfully compared with the experimental results available in the literature. The general nature of the model and the associated parametric study will be useful for the electrohydrodynamic (EHD) pumping in a micro-heat pipe. The present study can be extended to study the effects of wettability and viscosity on the performance of a heat pipe and in designing of a heat pipe.

Acknowledgement

Author thanks Kiran Mishra for her help in the manuscript preparation.

References

[1] P. Mracek, Application of micro heat pipe to laser diode cooling, Annual report of the VUMS, Prague, Czechoslovakia, 1988.
[2] G.P. Peterson, Heat pipes in the thermal control of electronic components, in: Proceedings of the 3rd International Heat Pipe Symposium, Tsukuba, Japan, September 12–14, 1988.
[3] G.P. Peterson, Heat removal key to shrinking avionics, Aerospace Amer. 8 (October) (1987) 20–22.
[4] Anonymous, Application of micro heat pipe in hyperthermia, Annual report of the Itoh R and D Laboratory, Osaka, 1989.
[5] G.P. Peterson, An Introduction to Heat Pipes, Wiley, New York, 1994 (Chapters 3 and 6).
[6] A. Faghri, Heat Pipe Science and Technology, Taylor and Francis, Washington, DC, 1995 (Chapter 10).
[7] J. Alario, R. Haslett, R. Kosson, The monogroove high performance heat pipe, AIAA paper 81-1156, June 1981.
[8] B.R. Babin, G.P. Peterson, D. Wu, Steady state modeling and testing of a micro heat pipe, J. Heat Transfer 112 (1990) 595–601.
[9] J.E. Beam, E.T. Mahafekey, Heat transfer visualization in the double wall artery heat pipe, in: AIAA/ASME Thermophysics and Heat Transfer Conference, Boston, MA, June 2–4, 1986.
[10] D.D. Stalmach, J.A. Oren, R.L. Cox, Systems evaluation of thermal bus concepts, 2-53200/2r-53030, Vought Crop. Dallas, TX, February 1984.
[11] G.L. Fleischman, Osmotic heat pipe, Air Force Wright Aeronautical Lab., TR-81-31332, Wright-Patterson AFB, Dayton, OH, November 1982.
[12] T. Narasaki, The characteristics of bimorph vibrator pump, in: Proceedings of the SAE Energy Conservation Engineering Conference, San Franscisco, CA, August 1978, pp. 2005–2010.
[13] G.P. Peterson, Thermal control systems for spacecraft instrumentation, J. Spacecraft Rockets 24 (1) (1986) 7–14.
[14] A.J. Hanford, M.K. Ewert, Advanced active thermal control systems architecture study, NASA TM 104822, Houston, TX, October 1996.
[15] T.P. Cotter, Principles and prospects of micro heat pipes, in: Proceedings of the 5th International Heat Pipe Conference, Tsukuba, Japan, 328–332, 1984.
[16] J.M. Ha, G.P. Peterson, Analytic prediction of axial dry-out point for evaporating liquids in axial microgrooves, J. Heat Transfer 120 (1998) 452–457.
[17] D. Khrustalev, A. Faghri, Thermal analysis of a micro heat pipe, J. Heat Transfer 116 (1) (1994) 189–198.
[18] D. Khrustalev, A. Faghri, Thermal characteristics of conventional and flat miniature axially grooved heat pipes, J. Heat Transfer 117 (1995) 1048–1054.
[19] H.B. Ma, G.P. Peterson, Experimental investigation of the maximum heat transport in triangular grooves, J. Heat Transfer 118 (1996) 740–746.
[20] G.P. Peterson, H.B. Ma, Theoretical analysis of the maximum heat transport in triangular grooves: a study of idealized micro heat pipe, J. Heat Transfer 118 (1996) 731–739.
[21] L.W. Swanson, G.C. Herdt, Model of the evaporative meniscus in a capillary tube, J. Heat Transfer 114 (1992) 434–441.

[22] L.W. Swanson, G.C. Herdt, The interfacial thermodynamics of micro heat pipes, J. Heat Transfer 115 (1995) 195–201.
[23] J.M. Ha, G.P. Peterson, Analytical prediction of axial dry-out point for evaporating liquids in axial microgrooves, J. Heat Transfer 120 (1998) 452–457.
[24] S. Anand, S. De, S. DasGupta, Experimental and theoretical study of axial dry-out point for evaporative from V-shaped microgrooves, Int. J. Heat Mass Transfer 45 (2002) 1535–1543.
[25] I. Catton, G.R. Stroes, A semi-analytical model to predict the capillary limit of heated inclined triangular capillary grooves, J. Heat Transfer 124 (2002) 162–168.
[26] B. Suman, S. De, S. DasGupta, A Model of the capillary limit of a micro grooved heat pipe and the prediction of dry out length, Int. J. Heat Fluid Flow 26 (3) (2005) 495–505.
[27] B. Suman, S. De, S. DasGupta, Transient modeling of micro-grooved heat pipe, Int. J. Heat Mass Transfer 48 (8) (2005) 1633–1646.
[28] B. Suman, N. Hoda, Effect of variations in thermophysical properties and design parameters on the performance of a V-shaped micro grooved heat pipe, Int. J. Heat Mass Transfer 48 (2005) 2090–2101.
[29] B. Suman, P. Kumar, An analytical model for fluid flow and heat transfer in a micro heat pipe of polygonal shape, Int. J. Heat Mass Transfer 48 (2005) 4498–4509.
[30] T.B. Jones, An electrohydrodynamic heat pipe, Mech. Eng. 96 (1) (1974) 27–32.
[31] T.B. Jones, M.P. Perry, Electrohydrodynamic heat pipe experiments, J. Appl. Phys. 45 (5) (1974) 2129–2132.
[32] R.I. Loehrke, R.J. Debs, Measurements of the performance of an electrohydrodynamic heat pipe, AIAA Paper 75-659, May 1975.
[33] M.K. Bologa, I.K. Savin, Electrohydrodynamic Heat Pipes, in: Proceedings of the 7th International Heat Pipe Conference (Minsk), Begell House, New York, 1990, pp. 549–562.
[34] B.R. Babin, G.P. Peterson, J. Seyed-Yagoobi, Experimental investigation of an ion-drag pump assisted heat pipe, J. Thermophys. Heat Transfer 7 (2) (1993) 340–345.
[35] M. Sato, S. Nishida, F. Noto, Study on electrohydrodynamical heat pipe, in: ASME JSES KSES International Solar Energy Conference, Part 1 of 2, American Society of Mechanical Engineers, New York, 1992, pp. 155–160.
[36] J.R. Melcher, Electric field and moving media, IEEE Trans. Educ. E-17 (2) (1974) 100–110.
[37] J.E. Bryan, J. Seyed-Yagoobi, Heat transport enhancement of monogroove heat pipe with electrohydrodynamic pumping, J. Thermophys. Heat Transfer 11 (3) (1997) 454–460.
[38] K.P. Hallinan, W.W. Bhagat, B. Kashaboina, R. Kashani, Electrohydrodynamic Augmentation of Heat Transport in Micro Heat Pipe Arrays, HTD vol. 361-3, American Society of Mechanical Engineers, Anaheim, CA, 1998, pp. 165–171.
[39] Z.Q. Yu, K. Hallinani, W. Bhagat, R. Kashani, Electrohydrodynamically augmented micro heat pipes, J. Thermophys. Heat Transfer 16 (2) (2002) 180–186.
[40] Z. Yu, P.H. Kelvin, P. Kashani, Temperature control of electrohydrodynamic micro heat pipe, Exp. Thermal Fluid Sci. 27 (2003) 867–875.
[41] J.R. Melcher, Continuum Electromechanics, MIT Press, Cambridge, MA, 1981.
[42] M. Ravikumar, S. DasGupta, Modeling of evaporation from V-shaped microgrooves, Chem. Eng. Commun. 160 (1997) 225–248.
[43] J.M. Crowley, Fundamentals of Applied Electrostatics, Wiley, New York, 1986, pp. 19, 20, 161–167.
[44] B. Suman, On the fill-charge and the sensitivity analysis of a V-shaped micro heat pipe, AICHE J., submitted for publication.
[45] H.B. Ma, G.P. Peterson, The minimum meniscus radius and capillary heat transport limit in micro heat pipes, J. Heat Transfer 120 (1998) 227–233.
[46] P.S. Ayyaswamy, I. Catton, D.K. Edwards, Capillary flow in triangular grooves, ASME J. Appl. Phys. 41 (1974) 332–336.
[47] S.W. Chi, Heat Pipe Theory and Practice, McGraw-Hill, New York, 1982.